

Flying couplers above spinning resonators generate irreversible refraction

Shai Maayani^{1,7}, Raphael Dahan^{1,7}, Yuri Kligerman¹, Eduard Moses^{1,2}, Absar U. Hassan³, Hui Jing⁴, Franco Nori^{5,6}, Demetrios N. Christodoulides³ & Tal Carmon^{1*}

Creating optical components that allow light to propagate in only one direction—that is, that allow non-reciprocal propagation or ‘isolation’ of light—is important for a range of applications. Non-reciprocal propagation of sound can be achieved simply by using mechanical components that spin^{1,2}. Spinning also affects de Broglie waves³, so a similar idea could be applied in optics. However, the extreme rotation rates that would be required, owing to light travelling much faster than sound, lead to unwanted wobbling. This wobbling makes it difficult to maintain the separation between the spinning devices and the couplers to within tolerance ranges of several nanometres, which is essential for critical coupling^{4,5}. Consequently, previous applications of optical^{6–17} and optomechanical^{10,17–20} isolation have used alternative methods. In hard-drive technology, the magnetic read heads of a hard-disk drive fly aerodynamically above the rapidly rotating disk with nanometre precision, separated by a thin film of air with near-zero drag that acts as a lubrication layer²¹. Inspired by this, here we report the fabrication of photonic couplers (tapered fibres that couple light into the resonators) that similarly fly above spherical resonators with a separation of only a few nanometres. The resonators spin fast enough to split their counter-circulating optical modes, making the fibre coupler transparent from one side while simultaneously opaque from the other—that is, generating irreversible transmission. Our setup provides 99.6 per cent isolation of light in standard telecommunication fibres, of the type used for fibre-based quantum interconnects²². Unlike flat geometries, such as between a magnetic head and spinning disk, the saddle-like, convex geometry of the fibre and sphere in our setup makes it relatively easy to bring the two closer together, which could enable surface-science studies at nanometre-scale separations.

The real part of the refractive index of a material describes the speed of light in that material on the basis of linear light–matter interaction. An irreversible refractive index²³ was originally demonstrated by Fizeau in flowing water, in an experiment of paramount importance for the development of special relativity. Such an irreversible index has generally been considered in photonics only when the entire apparatus, including its detector and emitter, is moving (such as in gyroscopes). Controlling photonic structures in such a way that they exhibit an irreversible index is challenging, as is controlling rapidly moving dielectrics while self-positioning them with nanometre precision. Therefore, current photonic technology and fundamental studies that involve light generally use stationary, non-self-positioned dielectrics and rely on a reversible index that treats counter-propagating light equally. Here we report a photonic device containing a dielectric material that moves sufficiently fast, while its position is self-adjusted finely enough, to achieve an irreversible index, which either passes or blocks light depending on the direction it comes from.

We fabricate a spherical resonator by melting the end of a silica-glass cylinder, flame-polishing it and then mounting the resonator on a turbine (Fig. 1d, Methods). In our experimental setup

(Fig. 1), this rotating silica sphere, which is resonant when its circumference corresponds to an integer number of optical wavelengths, is positioned near a tapered region of a standard single-mode telecommunications fibre. This tapered region is used to couple light evanescently^{4,5} into the rotating resonator. In the same manner, light is coupled out through the other side of the fibre via the same coupler. Each side of the fibre thus serves simultaneously as both an input port and an output port. Depending on the input port, light is coupled to circulate in the sphere in either the clockwise or the anticlockwise direction. Because of the Fizeau drag, the refractive index that light experiences in the spinning dielectric sphere is different in these counter-circulating directions. As a result, light entering from one side of the fibre is on resonance and is critically absorbed^{4,5}, whereas light entering from the other side is off resonance and so is almost 100% transmitted.

Central to the realization of such an irreversible index are the aerodynamic processes at play when the nanoscale fibre is only a small distance above the rapidly spinning spherical resonator. Numerical calculations (Methods; Fig. 2d) demonstrate that, for a sphere spinning at an angular velocity Ω , a boundary layer of air forms that is dragged past the stationary taper. By dragging the air into the region between the taper and the sphere, the moving sphere causes the taper to fly at a height h above the sphere, owing to the air pressure on the surface of the taper that faces the sphere (the ‘air bearing’ surface). If any perturbation causes the taper to rise higher than this stable-equilibrium height, it floats back to its original position; we refer to this behaviour as ‘self-adjustment’.

As shown in Methods, the tension of the taper, T , can be estimated analytically from

$$T = 6.19\mu R^{5/2}\Omega \int_0^r (h - \sqrt{r^2 - x^2} + r)^{-3/2} dx \quad (1)$$

where μ is the viscosity of air, r is the radius of the taper and R is the radius of the sphere. When operating at tensions near 3 GPa²⁴, we find $h = 320$ nm and $h = 38.2$ nm for the cases shown in Figs. 2 and 3, respectively. The self-adjustment of the taper separation from the rotating sphere enables critical coupling^{4,5} of light into the sphere, whereby counter-circulating light experiences optical drag identical in size, but opposite in sign.

To understand how Fizeau drag leads to isolation, we first take into account the relativistic addition of velocities when the periphery of the rotating silica resonator is moving towards or away from the input/output ports where the light coupling takes place (Fig. 1). On the basis of these considerations, we conclude that, in the laboratory frame, the refractive indices associated with the clockwise (+) and anticlockwise (−) whispering-gallery modes are $n_{\pm} = n[1 \pm v(n^2 - 1)/c]$, where n is the refractive index of silica, c is the speed of light in vacuum, $v = R\Omega$ is the tangential velocity of the rotating optical cavity and R is the radius of the resonator.

¹Faculty of Mechanical Engineering, Technion, Haifa, Israel. ²J-Rom, Haifa, Israel. ³CREOL/College of Optics and Photonics, University of Central Florida, Orlando, FL, USA. ⁴Physics Department, Hunan Normal University, Changsha, China. ⁵Physics Department, University of Michigan, Ann Arbor, MI, USA. ⁶Theoretical Quantum Physics Laboratory, RIKEN Cluster for Pioneering Research, Wako-shi, Japan. ⁷These authors contributed equally: Shai Maayani, Raphael Dahan. *e-mail: tcarmon@technion.ac.il

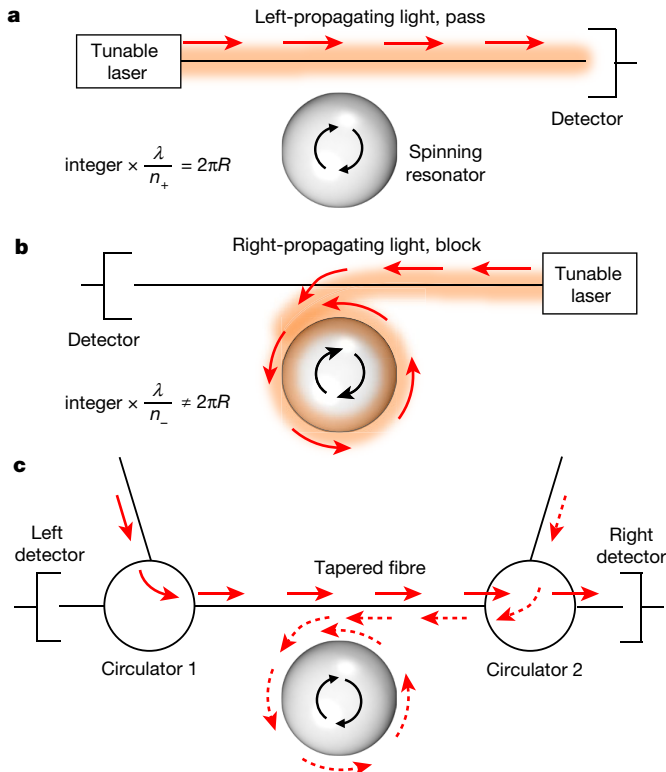
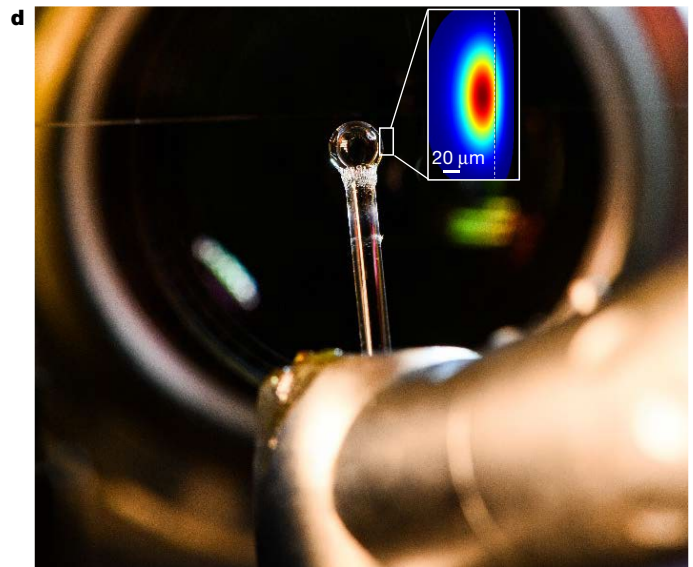


Fig. 1 | Experimental setup. Spinning the silica sphere (the resonator) results in different refractive indices for the counter-circulating whispering-gallery modes of the resonator. **a**, **b**, Illustration of the left-propagating ‘pass’ configuration (**a**) and the right-propagating ‘block’ configuration, where the input light does not match the resonance frequency of the cavity (**b**). **c**, The setup enables us to perform experiments in which light enters from both ports simultaneously. Solid (dashed) arrows represent the path of the transmitted (blocked) light.



In the blocked path, the light is absorbed in the resonator and does not reach the detector. **d**, A micrograph of our experimental setup; the inset shows the calculated transverse field of the optical resonance. Optical polarization in our scheme is either parallel or perpendicular to the rotation axis of the sphere, compatible with the polarization of the transverse electric or the transverse magnetic mode of the sphere. This polarization does not affect the performance when we use our polarized light source.

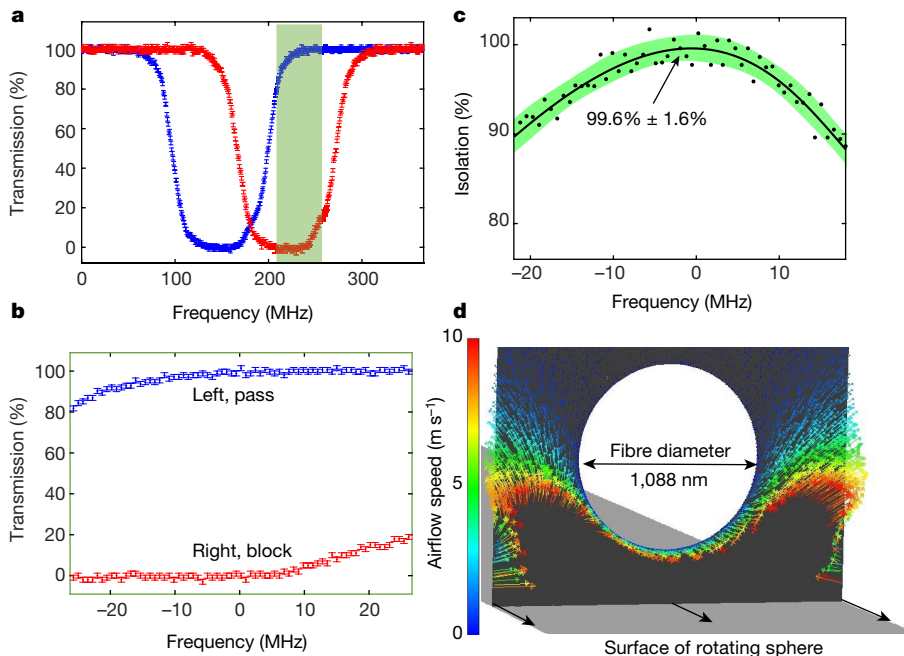


Fig. 2 | Experimentally measured isolation of 99.6%. **a**, **b**, Optical transmission of light coming simultaneously from the left (red) and right (blue) while scanning the laser frequency. The frequency range shown in **b** corresponds to the region shaded green in **a**, with 0 MHz corresponding to the centre of this region. The error bars show the standard deviation. **c**, Experimentally measured isolation (circles) and theoretical fit (line; see Methods); the green shading shows the confidence band for the fit.

The curve peaks at a maximum isolation of $99.6\% \pm 1.6\%$. **d**, The airflow near the fibre (arrows represent calculated direction; colour represents calculated speed) pushes the taper (empty circle) away from the interface of the rotating sphere (grey surface at the bottom). For this experiment, the optical wavelength is $\lambda = 1.55\ \mu\text{m}$, the radius of the resonator is $R = 4.75\ \text{mm}$ and its rotation frequency is $\Omega = 2\pi \times 3,000\ \text{rad s}^{-1}$.

The difference in resonance frequency between the counter-circulating modes is then²⁵

$$\Delta\omega_F = 2\omega_{\text{rest}} \frac{nR\Omega}{c} \left(1 - \frac{1}{n^2} - \frac{\lambda}{n} \frac{dn}{d\lambda} \right) = \eta\Omega \quad (2)$$

where ω_{rest} is the optical resonance frequency for a stationary resonator and λ is the optical wavelength in vacuum. Scattering between counter-circulating modes²⁶ is eliminated in our experiments to prevent unwanted reflections (see Methods). In addition, the coupling is set to critical^{4,5} to prevent transmission in the wrong direction. Under these conditions, and taking into account the frequency shift from equation (2), the rate equations²⁷ for the counter-circulating modes, with field amplitudes a_{\circlearrowleft} and a_{\circlearrowright} , are

$$\begin{aligned} \dot{a}_{\circlearrowleft} + \left[\frac{t^2}{\tau} + i(\omega - \omega_{\text{rest}} + \eta\Omega) \right] a_{\circlearrowleft} &= i \frac{t}{\tau} \vec{a}_{\text{in}}, & \vec{a}_{\text{out}} &= \left(1 - \frac{t^2}{2} \right) \vec{a}_{\text{in}} + ita_{\circlearrowleft} \\ \dot{a}_{\circlearrowright} + \left[\frac{t^2}{\tau} + i(\omega - \omega_{\text{rest}} - \eta\Omega) \right] a_{\circlearrowright} &= i \frac{t}{\tau} \vec{a}_{\text{in}}, & \vec{a}_{\text{out}} &= \left(1 - \frac{t^2}{2} \right) \vec{a}_{\text{in}} + ita_{\circlearrowright} \end{aligned} \quad (3)$$

where ω is the optical frequency of the input light, t is the real amplitude coefficient of transmittance between the fibre and the resonator, τ is the circulation time for the mode travelling inside the sphere, \vec{a}_{in} (\vec{a}_{in}) is the optical input from the left (right) and \vec{a}_{out} (\vec{a}_{out}) is the optical output from the right (left). Accordingly, the optical transmission for the opposing directions are

$$\begin{aligned} \vec{T} &= \left| \frac{\vec{a}_{\text{out}}}{\vec{a}_{\text{in}}} \right|^2 = 1 - \frac{t^4}{t^4 + \tau^2(\omega - \omega_{\text{rest}} + \eta\Omega)^2} \\ \overleftarrow{T} &= \left| \frac{\overleftarrow{a}_{\text{out}}}{\overleftarrow{a}_{\text{in}}} \right|^2 = 1 - \frac{t^4}{t^4 + \tau^2(\omega - \omega_{\text{rest}} - \eta\Omega)^2} \end{aligned} \quad (4)$$

Equation (4) clearly indicates that the transmission in this rotating resonator system is non-reciprocal: the equations are identical, except for the sign of η , which facilitates isolation by resonantly absorbing light entering from one side, while off-resonantly transmitting the counter-propagating light. Importantly, the equations in equation (3) are uncoupled because \vec{a}_{out} is not a function of $\overleftarrow{a}_{\text{in}}$ and $\overleftarrow{a}_{\text{out}}$ is not a function of \vec{a}_{in} , which allows crosstalk-free operation while light enters simultaneously from both sides.

We measured the spectral transmission as a function of the input direction (Fig. 2) and as a function of rotation speed (Fig. 3). In the first experiment, we demonstrate that our isolator almost completely transmits light coming from one side of the fibre while blocking light coming from the other side. As expected from equation (4), tuning the laser frequency ω through the counter-circulating resonance frequencies, $\omega_{\text{rest}} - \eta\Omega$ and $\omega_{\text{rest}} + \eta\Omega$, reveals oppositely drifted dips in transmission in for the two opposing directions (Fig. 2a). The split between these counter-circulating modes is larger than their widths, which enables light from one side to pass through while the other side is blocked (Fig. 2b). Isolation is most challenging when light enters from both sides of the isolator at the same time, because the isolator might suffer from both imperfect transmission of one beam and backscattering of the other.

To measure the degree of isolation, we subtract the power of light in the blocking direction (ideally 0%; red, Fig. 2b) from the power of light in the transmitting direction (ideally 100%; blue, Fig. 2b), while injecting light to the isolator from both sides (Fig. 1c). As can be seen in Fig. 2c, we measure a remarkable 99.6% intra-fibre isolation (Methods), despite the challenge of simultaneous two-port input.

In the second experiment, we measure the frequency shift as a function of the mechanical rotation rate (Fig. 3). Starting from rest ($\Omega = 0$) as a control experiment, the counter-circulating modes overlap, owing to their expected degeneracy (Fig. 3b). As predicted by equation (2),

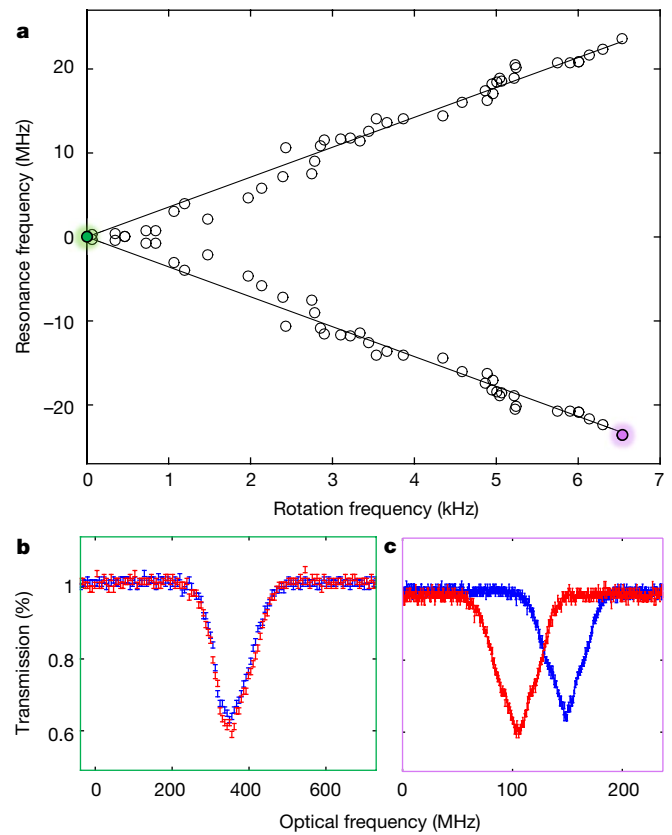


Fig. 3 | The Fizeau shift. **a**, The Fizeau shift is evident from the split between the counter-circulating resonances as a function of the rotation speed of the resonator. Circles describe experimental results and solid lines represent linear fits. **b**, **c**, Transmission spectrum in a control experiment while the resonator is at rest (**b**; corresponding to the green shaded point in **a**) and while the resonator is spinning at 6.6 kHz (**c**; purple shaded point in **a**). The experimental setup is shown in Fig. 1. The radius of the sphere is $R = 1.1$ mm. Red (blue) data points are for transmission of light coming from the right (left). The error bars are one standard deviation.

increasing the mechanical rotation frequency Ω results in a linear opposing frequency shift of $\eta\Omega$ (Fig. 3a) for the counter-circulating modes.

In conclusion, we have demonstrated optical non-reciprocity experimentally by breaking time-reversal symmetry through a mechanically spinning optical resonator. In addition, enabling intra-fibre isolation could be beneficial for applications such as fibre-linked quantum photon routings²². We believe that our work can be extended to spinning microphotonics, with similar nanometre-scale flying heights. When approaching couple-resonator separations of 300 fm^{28} (a regime related to femtotechnology), repulsive van der Waals forces are predicted to start acting against the large Casimir attraction²⁸. Being highly convex, spheres might be ideal for testing exceptionally small separation distances, near the boundary between the compliant surfaces. Furthermore, with the availability of quadrant photodiodes for highly accurate measurements in optical tweezers, tweezed counter-rotating spheres, one flying the other, might allow tests of gravity at distances shorter than what the current state-of-the-art permits. Although challenging, miniaturization and faster spinning of our resonators might be possible with continual technological improvements in the rotation²⁹ and manipulation³⁰ of spherical dielectrics.

Online content

Any Methods, including any statements of data availability and Nature Research reporting summaries, along with any additional references and Source Data files, are available in the online version of the paper at <https://doi.org/10.1038/s41586-018-0245-5>.

Received: 2 November 2017; Accepted: 17 April 2018;
Published online 27 June 2018.

1. Fleury, R., Sounas, D. L., Sieck, C. F., Haberman, M. R. & Alù, A. Sound isolation and giant linear nonreciprocity in a compact acoustic circulator. *Science* **343**, 516–519 (2014).
2. Yang, Z. et al. Topological acoustics. *Phys. Rev. Lett.* **114**, 114301 (2015).
3. Hasselbach, F. & Nicklaus, M. Sagnac experiment with electrons: observation of the rotational phase shift of electron waves in vacuum. *Phys. Rev. A* **48**, 143–151 (1993).
4. Dubreuil, N. et al. Eroded monomode optical fiber for whispering-gallery mode excitation in fused-silica microspheres. *Opt. Lett.* **20**, 813–815 (1995).
5. Spillane, S. M., Kippenberg, T. J., Painter, O. J. & Vahala, K. J. Ideality in a fiber-taper-coupled microresonator system for application to cavity quantum electrodynamics. *Phys. Rev. Lett.* **91**, 043902 (2003).
6. Chang, L. et al. Parity-time symmetry and variable optical isolation in active-passive-coupled microresonators. *Nat. Photon.* **8**, 524–529 (2014).
7. Gallo, K., Assanto, G., Parameswaran, K. R. & Fejer, M. M. All-optical diode in a periodically poled lithium niobate waveguide. *Appl. Phys. Lett.* **79**, 314–316 (2001).
8. Ibrahim, S. K., Bhandare, S., Sandel, D., Zhang, H. & Noe, R. Non-magnetic 30 dB integrated optical isolator in III/V material. *Electron. Lett.* **40**, 1293–1294 (2004).
9. Yu, Z. & Fan, S. Complete optical isolation created by indirect interband photonic transitions. *Nat. Photon.* **3**, 91–94 (2009); corrigendum 3, 303 (2009).
10. Kang, M. S., Butsch, A. & Russell, P. S. J. Reconfigurable light-driven opto-acoustic isolators in photonic crystal fibre. *Nat. Photon.* **5**, 549–553 (2011).
11. Lira, H., Yu, Z., Fan, S. & Lipson, M. Electrically driven nonreciprocity induced by interband photonic transition on a silicon chip. *Phys. Rev. Lett.* **109**, 033901 (2012).
12. Fan, L. et al. An all-silicon passive optical diode. *Science* **335**, 447–450 (2012).
13. Poulton, C. G. et al. Design for broadband on-chip isolator using stimulated Brillouin scattering in dispersion-engineered chalcogenide waveguides. *Opt. Express* **20**, 21235–21246 (2012).
14. Hafezi, M. & Rabl, P. Optomechanically induced non-reciprocity in microring resonators. *Opt. Express* **20**, 7672–7684 (2012).
15. Peng, B. et al. Parity-time-symmetric whispering-gallery microcavities. *Nat. Phys.* **10**, 394–398 (2014).
16. Lu, L., Joannopoulos, J. D. & Soljačić, M. Topological photonics. *Nat. Photon.* **8**, 821–829 (2014).
17. Shen, Z. et al. Experimental realization of optomechanically induced non-reciprocity. *Nat. Photon.* **10**, 657–661 (2016).
18. Kim, J., Kim, S. & Bahl, G. Complete linear optical isolation at the microscale with ultralow loss. *Sci. Rep.* **7**, 1647 (2017).
19. Fang, K. et al. Generalized non-reciprocity in an optomechanical circuit via synthetic magnetism and reservoir engineering. *Nat. Phys.* **13**, 465–471 (2017).
20. Ruesink, F., Miri, M.-A., Alù, A. & Verhagen, E. Nonreciprocity and magnetic-free isolation based on optomechanical interactions. *Nat. Commun.* **7**, 13662 (2016).
21. Gross, W. A. *Gas Film Lubrication* (Wiley, New York, 1962).
22. Shomroni, I., Rosenblum, S., Lovsky, Y. & Bechler, O. All-optical routing of single photons by a one-atom switch controlled by a single photon. *Science* **345**, 903–906 (2014).
23. Franke-Arnold, S., Gibson, G., Boyd, R. W. & Padgett, M. J. Rotary photon drag enhanced by a slow-light medium. *Science* **333**, 65–67 (2011).
24. Matthewson, M., Kurkjian, C. R. & Gulati, S. T. Strength measurement of optical fibers by bending. *J. Am. Ceram. Soc.* **69**, 815–821 (1986).
25. Malykin, G. B. The Sagnac effect: correct and incorrect explanations. *Phys. Uspekhi* **43**, 1229–1252 (2000).
26. Mazzei, A. et al. Controlled coupling of counterpropagating whispering-gallery modes by a single Rayleigh scatterer: a classical problem in a quantum optical light. *Phys. Rev. Lett.* **99**, 173603 (2007).
27. Gorodetsky, M. L. & Ilchenko, V. S. Optical microsphere resonators: optimal coupling to high-Q whispering-gallery modes. *J. Opt. Soc. Am. B* **16**, 147–154 (1999).
28. Li, J., Liu, B., Hua, W. & Ma, Y. Effects of intermolecular forces on deep sub-10 nm spaced sliders. *IEEE Trans. Magn.* **38**, 2141–2143 (2002).
29. Arita, Y., Mazilu, M. & Dholakia, K. Laser-induced rotation and cooling of a trapped microgyroscope in vacuum. *Nat. Commun.* **4**, 2374 (2013).
30. Grier, D. G. A revolution in optical manipulation. *Nature* **424**, 810–816 (2003).

Acknowledgements We thank U. Hofi, Z. Katz, Y. Halupovich and B. Khachatryan for their help. This work was funded by the Israeli Centers for Research Excellence (I-CORE), 'Circle of Light' Excellence Center, the Israel Science Foundation (2013/15), the Israel Ministry of Science, Technology and Space, the MURI Center for Dynamic Magneto-Optics via the AFOSR Award number FA9550-14-1-0040, the Army Research Office (ARO) under grant number 73315PH, the AOARD under grant number FA2386-18-1-4045, the CREST under grant number JPMJCR1676, the IMPACT programme of JST, the RIKEN-AIST Challenge Research Fund, the JSPS-RFBR under grant number 17-52-50023, and the Sir John Templeton Foundation.

Reviewer information *Nature* thanks A. Alù and M. Levy for their contribution to the peer review of this work.

Author contributions S.M. and R.D. performed the experiments. A.U.H., H.J., F.N., E.M., Y.K. and D.N.C. performed the theoretical analysis. T.C. supervised the work.

Competing interests The authors declare no competing interests.

Additional information

Extended data is available for this paper at <https://doi.org/10.1038/s41586-018-0245-5>.

Reprints and permissions information is available at <http://www.nature.com/reprints>.

Correspondence and requests for materials should be addressed to T.C.
Publisher's note: Springer Nature remains neutral with regard to jurisdictional claims in published maps and institutional affiliations.

METHODS

Backscattering and bandwidth. Our resonators have a relatively low optical quality factor ($Q < 10^6$), which results in a larger operation bandwidth and reduces unwanted backscattering.

Bandwidth. Low- Q resonators have broader resonance full-width at half-maxima and therefore improved bandwidth.

Backscattering. Backscattering typically appears in resonators with $Q \approx 10^8$, where absorption is reduced but scattering is still large. In such ultrahigh- Q resonators, frozen thermal capillary waves on the resonator solid-phase boundaries are created during reflow and scatter light later. Because our quality factor is relatively low ($Q < 10^6$) and probably governed by absorption rather than scattering, we did not observe any traces of backscattering in the spectrum of our rotating-resonator isolator (Fig. 2a, b). On the basis of the rotating-resonator isolation ratio (Fig. 2c), we conclude that imperfections in isolator performance, including those resulting from potential backscattering, are relevant to less than 0.2% of the input power. Although we do not exclude the possibility of backscattering effects in rotating-resonator isolators, in particular when the surface is rough, we did not observe such backscattering in our experiment.

Fabrication. We rotate a silica cylinder while its end is heated with a hydrogen-oxygen flame to reflow into a spherical shape. We did not attempt to increase the optical quality factor because it could have reduced the operation bandwidth of our isolator. For this reason, we use industrial-grade (rather than ultra-pure) gases for our flame.

Measuring and calculating isolation. Here we define isolation as the left-propagating (pass) transmission less the right-propagating (block) transmission. For the experimental results (black circles, Fig. 2c), the transmissions subtracted are those measured experimentally (Fig. 2a). For the theoretical fit (solid line, Fig. 2c), the subtracted transmissions are those revealed from fitting the experimental results (Fig. 2a) to equation (4).

The flying height. We observe experimentally that the taper does not touch the rotating resonator even if pushed towards it. Indications that the taper veers away from the spinning resonator when pushed towards it include our experimental observation that there is no wear of the taper or sphere, even after long periods of operation, and the fact that the taper does not stick to the rotating resonator, even when pushed towards it. By contrast, in a control experiment in which the sphere is stationary, the taper does stick to the sphere, through van der Waals forces, and needs to be pulled back to break the connection. Using a microscope, we then see micrometre-scale craters on the surfaces of the taper and the sphere, where contact was established. No such adhesion or abrasion is observed for the rotating-resonator case.

Fluid-film lubrication³¹ between surfaces provides a simple way to achieve the desired motion of a machine element with minimal friction and no wear. Such bearings have been studied for almost a century and found to be robust. In more detail, liquid- and gas-film²¹ lubrication have been studied for applications such as sand-proof bearings in marine vessels, dating back to 1932³², and have enabled flying heights of less than 10 nm in recently demonstrated helium-filled hard drives. Although such fliers are generally stable, modelling of them should consider effects such as lubricant compressibility and intermolecular forces.

Reynolds equation has previously been solved³³ with boundary conditions of a foil wrapping a rotating cylinder. Using similar methods, but with some modification³¹, the gap between the surface of the rotating cylinder and the foil was calculated to be

$$h = 0.643R^{5/3} \left(\frac{6\mu\Omega}{t'} \right)^{2/3} \quad (5)$$

where t' is the tension of the foil per unit width, R and Ω are the radius and angular velocity of the cylinder and μ is the viscosity of the fluid. In our case, the curvature of the sphere along the polar direction is so small compared with the width of the film-lubricated region of interest that it thins by only 1 Å by the end of this region. For this reason, we can estimate our rotating sphere using equation (5), even though it was originally developed for a rotating cylinder. Because equation (5) deals with flat foil, whereas our flyer is a wire, we break the circular cross-section of our wire into a set of infinitesimal flat stairs. We integrate the tension over these stairs to get the total tension T as a function of the minimum taper-sphere separation h (see equation (1)). Under typical operation at a fibre tensile stress near 3 GPa²⁴, equation (1) (with some corrections explained below) yields $h = 38.2$ nm for the sphere with $R = 1.1$ mm (Fig. 3) and $h = 320$ nm for the sphere with $R = 4.75$ mm (Fig. 2).

We now check the various assumptions of equation (1).

Intermolecular forces. It has been shown that effects such as Casimir and van der Waals forces begin to attract the flyer towards the rotor when the gap between them is reduced to less than 10 nm, and to strongly repel them when the gap is narrowed further, normally to below 300 fm²⁸. Taking intermolecular forces into account²⁸, equation (1) becomes

$$T = 6.19\mu R^{5/2}\Omega \int_0^r \left(\frac{1}{h - \sqrt{r^2 - x^2} + r} \right)^{3/2} dx + rR \left(-\frac{A}{6\pi h^3} + \frac{B}{45\pi h^9} - \frac{\pi^2 \hbar}{240h^4} \right) \quad (6)$$

where A and B are the Hamaker constants and \hbar is the reduced Planck constant. As expected, this intermolecular-force correction was found to be negligible in our experiment, with a contribution to the tension of less than 1% of the gas-lubricant contribution. Nonetheless, we do not exclude the possibility that such intermolecular forces might be relevant in future experiments, for example, when the rotation speed is reduced and the optical flyer is closer to the dielectric sphere.

Lubricant compressibility. We considered the effects of lubricant compressibility, using previously described methods³⁴, and found them to be relevant. In more detail, air was calculated to be up to 6.6 times denser at the lubrication region, requiring a correction of the constant in equation (1)³¹ (see Extended Data Table 1).

Tapered-fibre stiffness. We calculated the effects of the tapered-fibre stiffness, using a previously reported method³⁵, and found that they satisfy a condition that demonstrates the validity of equation (1).

Wrap angle. We calculated the effects of wrap angle, using a previously reported method³⁶, and found that they introduce a correction of less than 1% in the constant coefficient in equation (1).

Fluid inertia. We calculated the effects of fluid inertia were calculated, using a previously reported method³⁷, and found that they satisfy a condition that demonstrates the validity of equation (1).

Mean free pass. At a certain small scale, we can no longer consider air as a continuum and so have to consider the mean free path³⁷ between individual air molecules. This issue in the gas-film lubricant is treated here by using the Knudsen number, defined by the ratio between the flying height h and the mean free pass³¹.

For the case shown in Fig. 2, the Knudsen number is 0.13—corresponding to a regime in which continuous flow can be assumed and equation (1) needs no corrections.

For the case shown in Fig. 3, the Knudsen number is 1.4—corresponding to a regime in which free molecular flow effects should be taken into account. Calculating such flows requires a molecular-based model such as the Fukui-Kaneko model³⁸. Several other models for molecular gas-film lubrication have been reviewed³⁹ to provide an order-of-magnitude variation in results at this Knudsen number.

Numerically calculating the field flow. We calculate the airflow near the taper numerically using Ansys-Fluent software (<https://www.ansys.com>), assuming compressible flow.

Data availability. The data that support the findings of this study are available from the corresponding author on reasonable request.

- Gross, W. A. et al. *Fluid Film Lubrication* (John Wiley and Sons, New York, 1980).
- Busse, W. F. & Denton, W. H. Water-lubricated soft-rubber bearings. *Trans. Am. Soc. Mech. Eng.* **54**, 3–10 (1932).
- Blok, H. & Van Rossum, J. J. The foil bearing—a new departure in hydrodynamic lubrication. *Lubr. Eng.* **9**, 316–320 (1953).
- Eshel, A. Compressibility effects on the infinitely wide, perfectly flexible foil bearing. *J. Lubr. Technol.* **90**, 221–225 (1968).
- Eshel, A. & Elrod, H. G. Stiffness effects on the infinitely wide foil bearing. *J. Lubr. Technol.* **89**, 92–97 (1967).
- Langlois, W. E. The lightly loaded foil bearing at zero angle of wrap. *IBM J. Res. Develop.* **7**, 112–116 (1963).
- Jennings, S. G. The mean free path in air. *J. Aerosol Sci.* **19**, 159–166 (1988).
- Fukui, S. & Kaneko, R. Analysis of ultra-thin gas film lubrication based on linearized Boltzmann equation: first report—derivation of a generalized lubrication equation including thermal creep flow. *J. Tribol.* **110**, 253–261 (1988).
- Shen, S. & Chen, G. In *Encyclopedia of Tribology* (eds Wang, Q. J. & Chung, Y.-W.) 2309–2313 (Springer, New York, 2013).

Extended Data Table 1 | Effects of lubricant compressibility

Case	Lubricant compressibility [-]	Compressibility reduces the constant in equation (1) by	Flying height [nm]
Figure 2	6.6	56%	320
Figure 3	1.4	28%	38.2